Cerebral Cortex, March 2016;26: 991–1003

doi: 10.1093/cercor/bhu268
Advance Access Publication Date: 18 November 2014
Original Article

ORIGINAL ARTICLE

Functional Local Input to Layer 5 Pyramidal Neurons in the Rat Visual Cortex

Amir Zarrinpar[1,2,3] and Edward M. Callaway[1,2]

[1]Systems Neurobiology Laboratory, The Salk Institute for Biological Studies, La Jolla, CA 92037, USA, [2]Neurosciences Program, and [3]Current Address: Division of Gastroenterology, University of California, San Diego, La Jolla, CA 92093, USA

Address correspondence to Edward M. Callaway, Email: callaway@salk.edu

Abstract

Pyramidal neurons in layer 5 of the neocortex can be differentiated into 3 cell subtypes: 1) short regular spiking (SH), 2) tall regular spiking (TR), and 3) tall burst spiking (TB), based on their morphological and electrophysiological properties. We characterized the functional excitatory local input to these 3 cell subtypes in rat primary visual cortex using laser-scanning photostimulation. Although all cell types received significant input from all cortical layers, SH neurons received stronger input from layer 4 and weaker input from layer 5 than did tall pyramidal cells. However, the laminar input to the 2 populations of tall pyramidal cells was indistinguishable. Simultaneous paired recording were then used to calculate a correlation probability (CP) to infer the proportion of shared input based on the occurrence of simultaneous synaptic potentials. Tall pairs of matched type had significantly higher CPs compared with unmatched pairs, suggesting that subpopulations of layer 4, 5, and 6 neurons preferentially connect to each tall cell type. Hence, this study shows that unconnected but matching pairs of tall pyramidal neurons, but not short pyramidal neurons, receive functional input from different interconnected networks within layers 4, 5, and 6.

Key words: correlation probability, cortical circuitry, photostimulation, sensory systems, striate cortex

Introduction

Understanding the functional connectivity of cortical neurons is critical to deciphering how information processing occurs in the mammalian brain. Previous experiments have shown that each morphologically categorized cell type has highly specific connectivity (Mercer et al. 2005; Song et al. 2005; Kampa et al. 2006; Morishima and Kawaguchi 2006; West et al. 2006; Brown and Hestrin 2009; Morishima et al. 2011). As a result, each cell type receives specific functional input patterns that distinguishes it from other cell types (Dantzker and Callaway 2000; Schubert et al. 2001, 2003; Yoshimura and Callaway 2005; Yoshimura et al. 2005; Zarrinpar and Callaway 2006; Xu and Callaway 2009).

In studies of the rat sensory cortices, layer 5 pyramidal neurons have been until recently split into 2 groups based on either physiological (i.e., regular or burst spiking) or morphological characteristics (i.e., short or tall, slender, or thick dendrites). More recent studies of the layer 5 pyramidal neurons in the mouse somatosensory cortex show that there are 3 subtypes based on dendritic and axonal morphologies: short, tall simple, and tall tufted (Larsen and Callaway 2006; Larsen et al. 2007). Short pyramidal (SH) cells have apical dendrites that end before reaching layer 1. Their axons project to the superficial layers in a columnar fashion, and to the contralateral cortex. Tall simple cells have an apical dendrite with a tuft projecting into layer 1. Their axons project to the superficial layers with extensive lateral spread and to the contralateral cortex. Finally, tall tufted cells have an extensive dendritic tuft projecting widely in layer 1. Furthermore, they have axons that project almost exclusively to the deep layers, and to the superior colliculus and the thalamus. All 3 cell types are found throughout layer 5.

Earlier photostimulation experiments of the layer 5 pyramidal neurons in rat somatosensory cortex found no interlaminar, but subtle intercolumnar, differences when pyramidal neurons were split into regular-spiking (RS) and burst spiking cells (Schubert et al. 2001, 2006). We wondered if the results would be different in the visual cortex or if the RS cells were further split based on their dendritic morphologies. Furthermore, there may be subtle differences in functional input that can be detected by collecting photostimulation data from 2 cells simultaneously and analyzing their correlated input.

It is unclear whether the interconnected presynaptic networks feeding layer 5 cells that have been observed in other cortical areas exist in the rat visual cortex. These networks can be revealed by stimulating a small number of presynaptic neurons through photostimulation and analyzing their correlated input to pairs of layer 5 cells. This technique allows the evaluation of multiple inputs from different lamina, making it easier to understand cortical networks with fewer paired recordings.

This study had 2 main objectives: to characterize the neurons in layer 5 of the rat visual cortex based on both morphological and electrophysiological properties, and to use laser-scanning photostimulation to characterize the laminar organization of functional excitatory inputs and also correlated activity to these subtypes.

Materials and Methods

Slice Preparation

Vibratome-cut coronal slices (400 μm) were prepared from the primary visual cortex of P21–P28 Long-Evans rats of either sex. Slices were cut in ice cold oxygenated (95% O_2–5% CO_2) artificial cerebral spinal fluid (ACSF) [which contained (in mM) 125 NaCl, 5 KCl, 26 $NaHCO_3$, 1.25 KH_2PO_4, 1.33 $MgSO_4$, 10 D-(+)-glucose, 3.15 $CaCl_2$, and 1 kynurenic acid] and then maintained submerged in the same ACSF solution heated to 35–37°C. Since we are interested in having conditions which allows for good detection of evoked response (signal) above background levels of spontaneous currents (noise), we have used a higher concentration of $CaCl_2$ in our studies. In all slices, all layers provided significant laminar input to at least one of the cells we recorded from.

Electrophysiology

Slices were placed in submersion type chamber with continuous perfusion of oxygenated ACSF. We used an infrared Olympus DIC microscope with a ×40, 0.8 NA water-immersion lens to visualize and target layer 5 neurons for whole-cell recordings in living brain slices. Glass microelectrodes (5–10 MΩ resistance) filled with a potassium-gluconate-based intracellular solution (130 mM K-gluconate, 10 mM HEPES, 2 mM $MgCl_2$, 0.2 mM EGTA, 6 mM KCl, 2.5 mM Na_2ATP, 0.5 mM Na_2GTP, 10 mM K-phosphocreatine) contained 0.5%–1% biocytin for cell labeling. Recordings were made at room temperature. All intracellular recordings had access resistances of <20 MΩ. For each cell, we initially recorded in current clamp mode for spike shape analysis (see below) and then switched to voltage-clamp mode for measurement of evoked excitatory postsynaptic currents (EPSCs).

Photostimulation and Input Maps

Local stimulation of presynaptic input neurons by light-evoked conversion of "caged" glutamate to glutamate (photostimulation) was used to map laminar sources of functional connections onto individual recorded neurons (Supplementary Fig. 1) (Callaway and Katz 1993; Katz and Dalva 1994; Sawatari and Callaway 1996; Dantzker and Callaway 2000; Briggs and Callaway 2001, 2005; Yoshimura and Callaway 2005; Yoshimura et al. 2005; Zarrinpar and Callaway 2006). Brain slices were bathed in oxygenated ACSF (without kynurenic acid) containing ~85 μM "caged" glutamate (4-methoxy-7-nitroindolinyl-caged L-glutamate —"MNI-glutamate"; Tocris Biosciences, Ellisville, MO, USA) at room temperature. Ultraviolet light (10-ms flash from an argon-ion laser at ~200 mJ) was focused to photostimulate a small discrete spot in the plane of the brain slice through a ×40 microscope objective above the slice. Whole-cell voltage-clamp recordings (cell held at –65 mV) were made from 2 layer 5 postsynaptic neurons simultaneously, and inward EPSCs resulting from photostimulation of presynaptic neurons were measured. To map the location of input, ~600–800 sites were stimulated sequentially in a pseudo-random pattern that covered all cortical layers. Typically, each site is stimulated only once or twice. Stimulation sites were located throughout a rectangular area surrounding the recorded neuron, typically extending ~200–300 μm laterally on either side of the cell and vertically from the white matter to layer 1. After each photostimulation event, voltage-clamp records were made from each stimulation trial to detect EPSCs. In addition, photostimulation trials were interleaved with control trials (no stimulation) to obtain spontaneous EPSCs (sEPSCs). With each spontaneous recording access, resistance was checked to ensure that it had not changed as the experiment was progressing. After completion of photostimulation and recordings from a cell, the laser was used to burn alignment sites (<10 μm) into the slice so that *x*-*y* photostimulation coordinates could be assigned to their corresponding position in the tissue. Laminar borders were determined using cytochrome oxidase stain.

The spatial resolution of this technique allows mapping of laminar-specific excitatory input in rat visual cortex. Previously published spatial resolution experiments (Dantzker and Callaway 2000; Yoshimura and Callaway 2005; Yoshimura et al. 2005) show that, with the exception of layer 1, the locations of presynaptic neurons that are photostimulated to fire APs can be determined with an effective resolution of ~50 μm. Neurons only fire APs when directly stimulated, which rules out the possibility of polysynaptic APs from photostimulated neurons in other distant cortical layers. Furthermore, these studies indicate that presynaptic neurons fire multiple asynchronous APs when photostimulated, which increases the probability of detecting weak input to a postsynaptic cells. We supplemented previously published measures (Dantzker and Callaway 2000; Yoshimura and Callaway 2005; Yoshimura et al. 2005) with a series of experiments to assess the spatial resolution of the laser-scanning photostimulation with our given parameters. This was also to ensure that action potentials generated by glutamate uncaging occurred at similar distances to the cell bodies when compared between layers. Loose-patch extracellular recordings were made of cells throughout the cortical column (~3–5 cells in each layer). We recorded the frequency of action potentials after a photostimulation event and found that our results matched previously published experiments (Dantzker and Callaway 2000; Yoshimura and Callaway 2005; Yoshimoto et al. 2013); cells fired action potentials when focal uncaging occurred within ~50 μm from cell soma.

Staining and Morphological Analysis

After photostimulation, slices were fixed with 4% paraformaldehyde in 0.1 M PBS for 12–24 h, then submerged in 30% sucrose in PBS. The slices were then stained whole mount using a Cy3-conjugated streptavidin system (Jackson ImmunoResearch

Laboratories, Inc., West Grove, PA, USA). Slices were mounted using Vectashield (Vector Laboratories, Burlingame, CA, USA), and morphological characteristics of the cells were determined using confocal laser-scanning microscopy (TCS SP2 AOBS; Leica; see Fig. 1A). Multiple images of the cells were taken, including the whole cell with a low-resolution objective (PL Fluotar ×10; NA 0.3; Leica); the apical dendrites and cell bodies with a medium-resolution objective (PL Fluotar ×20; NA 0.5; Leica) and the cell bodies with a high-resolution objective (PLAN APO ×40; NA 0.85; Leica). Images were acquired as stacked files through the whole section thickness (step size, ~1 μm for ×10; ~0.5 μm for ×20, ~0.1 μm for ×40).

Slices were then resectioned at 80 μm, and stained for cytochrome oxidase and biocytin (see Fig. 1B) to reveal laminar borders and neuronal morphology using methods previously described (Yabuta and Callaway 1998a; 1998b). Cells that had an incomplete apical dendritic trunk, either because it was cut at the cell surface or it had poor staining, were excluded from all analyses. For all slices, the laminar borders near the cells were reconstructed with Neurolucida, a computerized system (MicroBrightField, Williston, VT, USA). The dendritic arbors of the cells were also reconstructed (see Fig. 1C). Each reconstruction showing the laminar borders and alignments sites was aligned with the coordinate map of stimulation sites using Adobe Illustrator (Adobe Systems, San Jose, CA). Each stimulation site was assigned to a layer using this method. However, photostimulation sites within 50 μm of the layer borders were excluded from analysis since they can stimulate presynaptic cells in 2 layers (Yoshimura and Callaway 2005; Yoshimura et al. 2005).

Analysis of EPSCs

We analyzed EPSCs that occurred during the first 150 ms after photostimulation. This window was chosen because presynaptic neurons fired most of their APs during this time (Dantzker and Callaway 2000; Yoshimura and Callaway 2005; Yoshimura et al. 2005), indicating that shorter analysis windows would exclude photostimulation-evoked EPSCs. We distinguished direct effects of focal uncaging of glutamate on the recorded cell, which invariably occurred within the 10-ms window from laser onset, had a distinct shape (longer rise-time), and occurred immediately after glutamate uncaging (shorter latency), and excluded them from our analysis (e.g., see Fig. 5E, trace 3). Currents that occur within the 10-ms window of laser onset are not synaptic since they occur before the generation of action potentials in photostimulated neurons. After photostimulation within ~50 μm of the recorded cell, direct currents sometimes exceeded 100 pA and decayed over 100 ms, preventing EPSCs from being separately identified at these locations, and thus these sites were excluded from analysis. The amplitudes and numbers of EPSCs were measured for every stimulation site and for the no-stimulation controls using peak analysis software from Synaptosoft (Leonia, NJ, USA) and other custom software. Each trial was assigned a value in picoamperes, equal to the sum of the peak amplitudes of all detectable EPSCs. Stimulation sites were then assigned to their correct cortical layer, and EPSC amplitudes for all stimulation sites within a layer were pooled together using custom Matlab programs. Laminar groupings of EPSC sum of amplitudes were then compared with spontaneous EPSCs to identify statistically significant differences in EPSCs from a particular layer using Mann–Whitney *U*-tests. We also calculated the mean value of summed EPSC amplitudes for that layer and also for control trials, measuring spontaneous EPSCs. To quantify the evoked input (EI) from a particular layer, the mean sum of amplitudes of spontaneous events was subtracted from the mean sum of evoked amplitudes all control trials. The relative strength of excitatory input from each layer was calculated by dividing the EI for that layer by the sum of the EIs from all layers for that same cell. Cells were then grouped based on their morphological characteristics. In addition, if a cell did not receive significant input from a layer, the EI for that layer was set to 0 to avoid negative EI and EI percentages. Significant differences in layer-specific EI percentages between cell types were determined using Mann–Whitney *U*-test. It should be noted that only EPSCs that were detectable at the soma (and hence can affect the axon hillock to generate an action potential) were measured. Because photostimulation excites multiple neurons, it is difficult to determine whether the EPSCs detected at the soma are from a proximal synapse on the soma, or from a summation of strong synapses from the distal dendrites. In other words, photostimulation does not allow one to distinguish the location of the synapse or the number of synapses that elicited an EPSC detected at the soma. Hence, only "functional" input to the cells, as opposed to all input, was analyzed.

To illustrate input patterns for individual cells, smoothed graphs of excitatory input were generated using custom Matlab programs. Values of the sum of amplitudes for each individual stimulation site were used to create these smoothed plots using linear interpolation. These plots illustrate estimated evoked activity measured in a given cell (mean sum of EPSC amplitudes for simulated trials minus mean sum of EPSC amplitudes for spontaneous trials) after stimulation at various locations. These plots are purely for illustration of the source of input; no part of the quantitative analyses was based on these linear interpolations.

Spike Analysis

An illustration of some of the spike analysis measurements that we made can be found in Supplementary Fig. 2. Recorded spike trains were analyzed off-line using custom software written in Igor Pro (Wavemetrics, Lake Oswego, OR, USA). Instantaneous firing rate (FR) was calculated as the reciprocal of the interspike interval and was assigned to all spikes except the first one in a train. To measure the FR, we injected all cells with the same amount of maximum current (200 pA) for 300 ms. We repeated this measure 20 or more times and averaged the firing frequency the cell attained. We calculated the adaptation coefficient which we defined as the ratio of the interspike interval of the penultimate pair of spikes to the last pair of spikes at the highest spiking frequency. Unless otherwise stated we did not use the first spike for each train in any of our analysis.

Action potential threshold was defined as the membrane potential at which the first derivative of the membrane potential (dV/dt) exceeded 10 V/s. Action potential height was defined from threshold to peak. Half peak width was calculated by measuring the width of the peak (in ms) at the point that was half the action potential height.

We calculated the time point at which the spike ended (end of spike, EOS) which we defined as the change in slope of the first derivative of the membrane potential (dV/dt) after the spike decreased by 90% (or when the postpeak maximum of the second derivative decreased by 90%). We also calculated an EOS potential (ΔEOS, in mV) by subtracting the threshold from the potential at which the spike ended. This value is positive if the spike is followed by a fast afterspike depolarization (ADP), and negative if the spike is followed with a fast afterspike hyperpolarization (AHP).

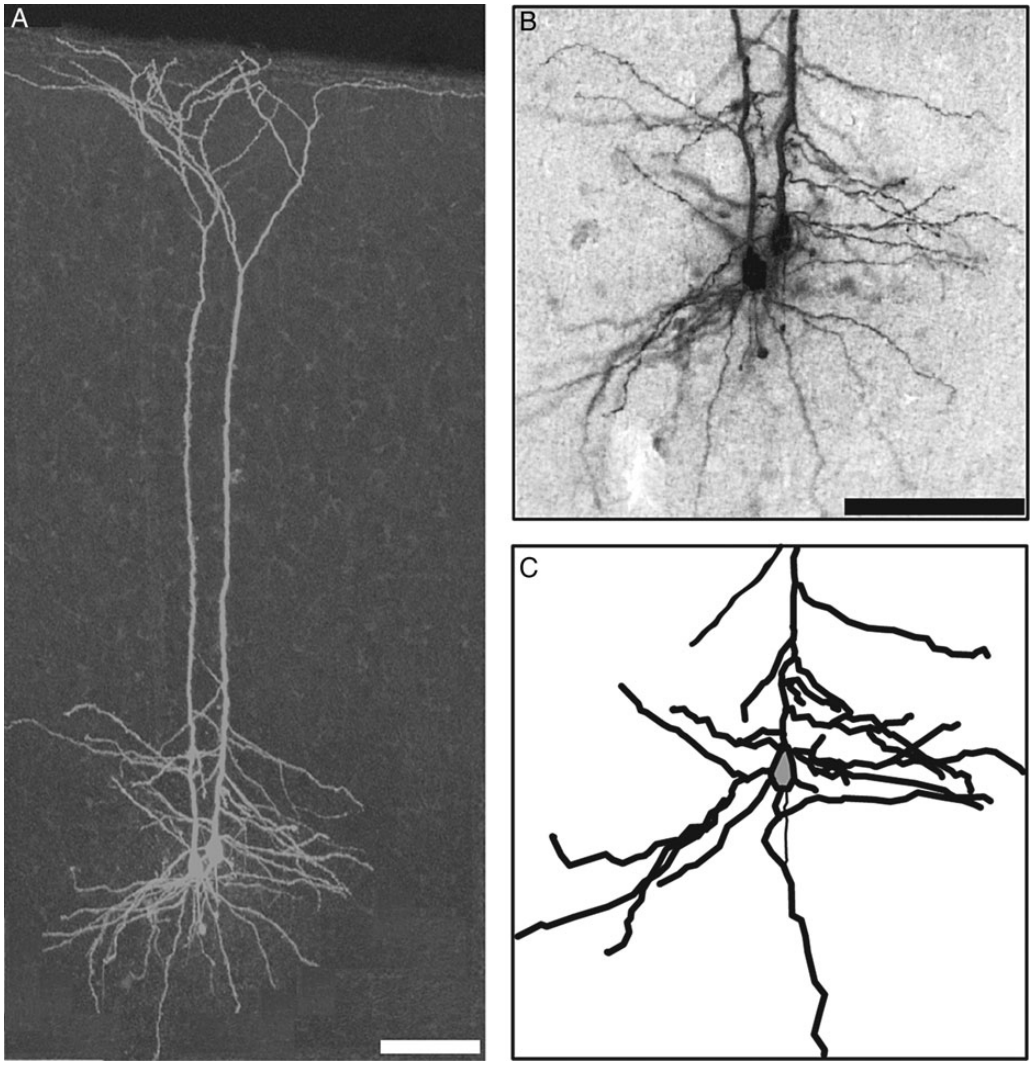

Figure 1. Staining and morphological analysis of cells. (*A*) A whole-cell image of a pair of cells from our study. This image was taken with a confocal laser-scanning microscope with a low-resolution objective (PL Fluotar ×10; NA 0.3; Leica). This image was acquired as stacked files through the whole section thickness (step size, ~1 µm for ×10). (*B*) Cytochrome oxidase and thionin-stained section containing a biocytin-labeled layer 5 pyramidal neurons depicted in (*A*). (*C*) Neurolucida reconstruction of the right cell in the pair depicted in (*A*) and (*B*). Dendrites are in dark black lines, soma is gray, and axon (which was not reconstructed) is the thin line. Scale bars are 200 µm.

We defined the moment of the AHP as the minimum between the 2 peaks ($dV/dt = 0$). AHP measurements for the last spike of a train were excluded from analysis. From this point, we calculated 2 AHP potentials: ΔAHP_1 is the membrane potential difference between the spike threshold and absolute membrane potential minimum between spikes; ΔAHP_2 is the membrane potential difference between the EOS and the absolute membrane potential minimum between spikes. In addition, an AHP time ratio (AHPtr) was calculated where the time interval between the AHP and the peak of the spike was divided by the interspike interval. A low ratio would imply that the AHP occurred very close to the spike, whereas a larger number implies that the AHP is delayed. AHPtr was not calculated for the last spike in a train.

Finally, we defined the ADP as the maximum between the EOS and AHP. It should be noted that spikes that had a fast ADP, and a high EOS (like some bursting cells) would sometimes have a value of 0 for ADP. This was mainly because the maximum between the EOS and AHP would be the EOS itself, causing EOS and ADP to be equal to each other, and their difference to be 0. The change in ADP potential (ΔADP) was calculated by subtracting EOS potential from the potential at the maximum between the EOS and AHP.

Cross-Correlation Analysis

We used established cross-correlation analysis methods (Aertsen et al. 1989; Yoshimura and Callaway 2005; Yoshimura et al. 2005) to normalize for synchrony resulting from time-locking of action potential generation to the stimulus (Supplementary Fig. 3). To obtain correlation probabilities, the number of synchronous synaptic currents attributable to shared input was expressed as a proportion of the total number of evoked synaptic currents for each cell. The correlation probability (CP) is an estimate of the probability that when a photostimulated presynaptic neuron fired an action potential and evoked a synaptic current in one of the 2 recorded layer 5 pyramidal cells, the same presynaptic neuron also evoked a synaptic current in the second recorded neuron. By calculating separate CPs based on stimulation sites in each cortical layer, we are able to determine the extent of

shared input from the different laminar sources to each pair of recorded layer 5 pyramidal cells.

Cross-correlograms of EPSCs were computed for each pair of simultaneously recorded layer 5 cells. Separate correlograms were computed for stimulation sites from each cortical layer (layers 2/3, 4, and 5). Cross-correlation data were binned into histograms using 4-ms bins; the central bin included values of 0 ± 2 ms. An optimal binning model was done with experimental and real variability in time difference. This model showed that the best central bin size was ±2 ms (hence, the reason why bin sizes are 4 ms). This is the same bin size as in previously published studies in our lab (Yoshimura and Callaway 2005; Yoshimura et al. 2005), which also rigorously tested bin size and also evaluated the distributions of measurable onset to peak times. The variability in times of onset to peak can be up to 2 ms, indicating that dendritic filtering and measurement error (difficulty identifying onset time) prevent the use of smaller bins. At any rate, the use of larger bins can slightly reduce the sensitivity of shared input estimates but would not lead to incorrect detection of shared inputs.

Data from stimulation trials (from the same layer) were also used to create shifted correlograms for each layer and cell pairs. To calculate the CP, the shifted correlogram was subtracted from the unshifted correlogram for the corresponding layer, and then the value in the central bin was divided by the average estimated total number of evoked EPSCs (for the 2 cells) observed for all trials in the relevant layer. The average number of evoked EPSCs was calculated as the total number of measured EPSCs for Cell A minus the expected number of spontaneous EPSCs for that cell, plus the same value calculated for Cell B. This total was then divided by 2.

Results

Cell Classification

We intracellularly labeled and performed spike analysis for 87 layer 5 neurons. Three cells had aspiny dendrites, local pervasive axonal projections, nonpyramidal somata, and distinct firing patterns and were classified as inhibitory interneurons and were excluded. The remaining 84 cells were split into 2 main groups based on cell morphology. Cells that did not have an apical dendrite that reached layer 1 were labeled SH neurons ($n = 16$; Fig. 2*A*), and cells that had dendritic tufts that extended into layer 1 were classified as tall pyramidal neurons ($n = 68$; Fig. 2*C*,*E*). All SH cells within this category were regular spiking (Fig. 2*B*), and were found throughout layer 5. The tall pyramidal neurons were further subdivided, based on electrophysiology, into bursting (TB) and regular spiking (TR) subgroups (Fig. 2*C*–*F*). There was no difference in the depth of the location of cells throughout layer 5 (Supplementary Fig. 4).

While performing this task, we came across 6 cells that had a fast ADP (high ΔEOS) that is characteristic of bursting cells though they did not show any bursting per se. Similar bursting cells have been described in previous literature (Chagnac-Amitai et al. 1990; Kasper et al. 1994). We initially analyzed the dataset without these cells and found that, besides the high ΔEOS, they shared many spike features with bursting cells, and were remarkably different from the TR cells (see below). Hence we reclassified these cells as TB cells. Hence, the final distribution included 16 SH neurons, 30 TR neurons, and 38 TB neurons.

Earlier studies of the layer 5 pyramidal cells in the somatosensory cortex found that tall cells can be further split into 2 groups based on diameters of the apical dendrite (Schubert et al. 2001; de Kock et al. 2007). In particular, cells that had an apical dendrite of <3 μm—slender tufted cells—had different response properties to whisker deflections and were characterized as regular-spiking.

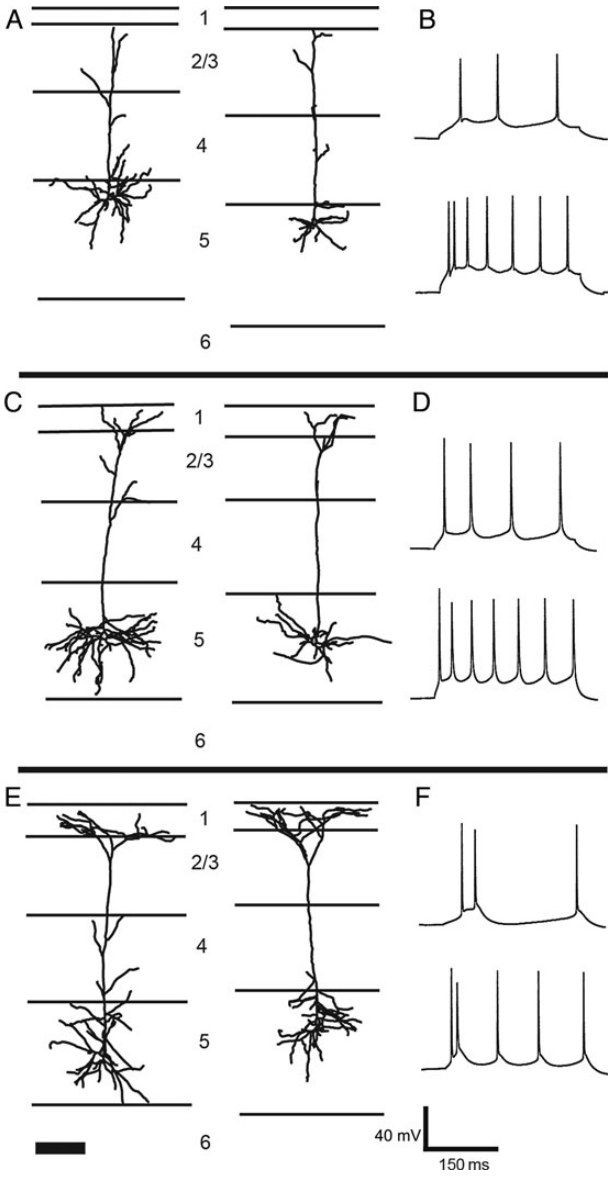

Figure 2. Examples of cell morphology of layer 5 pyramidal cells. Neurolucida drawing of 3 different neuron subtypes (with 2 examples each) differentiated based on dendritic morphology and cell spiking properties. Dark lines: dendrites; gray, somata. Axons have been excluded from the drawings. The sample traces are both from the same cell. Top traces are a response to a 100-pA current injection and the bottom trace is a response to 200-pA current injection. (*A*) Two examples of short pyramidal cells, identified by a lack of dendritic tuft and no dendritic branches or projections to layer 1. Although these 2 examples are from the top of layer 5, these cells were found throughout the entire cortex. (*B*) Sample spiking pattern from a short pyramidal cells. (*C*) Two examples of tall regular-spiking pyramidal neurons, classified by their morphological characteristics (dendritic tuft that projects to and branches in layer 1), slender apical dendrite, and spiking pattern (regular spiking). (*D*) Sample spiking pattern from a tall regular-spiking pyramidal cell. (*E*) Two examples of tall burst spiking pyramidal neurons, classified by their morphological characteristics (dendritic tuft that projects to and branches in layer 1), thick apical dendrite, and spiking pattern (burst spiking, followed by a fast afterspike depolarization). (*F*) Sample spiking pattern from a tall bursting cell. Scale bar in (*E*) represents 200 μm and applies to all drawings. Scale bars for the spike trains in (*F*) apply to all spike trains.

Those with thicker apical dendrites—thick tufted cells—were bursting pyramidal cells. Of the 68 tall cells in our study, the quality of cell labeling was suitable for accurate measurement of the apical dendritic diameters of 60 cells. Although the dendritic arborizations were preserved for the remaining 8 cells, the proximal dendrite reconstruction was incomplete, and, hence, they were excluded from this part of the analysis. We measured the apical dendrite at its most proximal end (at the most proximal of either the first dendritic spine or the first dendritic branch point). There was a significant difference between the apical dendrite thickness of TB (4.66 ± 0.23 μm; mean ± SEM) and TR cells (2.44 ± 0.07 μm; $P = 3.3 \times 10^{-9}$, Student's *t*-test). We found that 28 cells had an apical dendrite thickness that was <3 μm and 32 cells that were thicker than 3 μm (Fig. 3). All 32 cells that were thicker than 3 μm were TB cells. Furthermore, all but one of the 28 cells with an apical dendrite <3 μm were TR cells.

Spike Analysis

We characterized the electrophysiological characteristics of the different cell types to help aide their identification in future slice experiments. A summary of the spike features of the cell types is provided in Table 1 and sample cells in Fig. 4A–C.

The 3 cell types differed from each other the most along 2 variables, ΔEOS (EOS potential, see Materials and Methods) and the FR (see Materials and Methods). Of the 2, ΔEOS was the best at distinguishing TB cells from other cell types. TB cells had a ΔEOS of 2.377 ± 0.381 which was significantly higher than that of TR and SH cells ($P = 4.4 \times 10^{-8}$ and $P = 4.4 \times 10^{-8}$, respectively, Mann–Whitney *U*-test; Fig. 4C). Most of the TB cells had a ΔEOS >1 (n = 28/38, 74%) whereas only 3/30 (10%) of the TR spiking cells and none of the SH cells met this criteria ($P = 8.3 \times 10^{-11}$; Fisher's exact test, TB versus both SH and TR).

The cells with the highest FR were the SH cells (90.17 ± 4.34 Hz; Fig. 4A) which were significantly higher than the TR cells (29.32 ± 5.05 Hz; $P = 1.0 \times 10^{-6}$, Mann–Whitney *U*-test; Fig. 4B) and the TB cells (63.350 ± 4.81 Hz, $P = 1.0 \times 10^{-3}$, Mann–Whitney *U*-test; Fig. 4C). The TB cells had a faster FR than the TR cells ($P = 4.1 \times 10^{-6}$; Mann–Whitney *U*-test). A large majority of the TR cells (n = 26/30; 87%) had a FR lower than 40 Hz, whereas only 10/38 (26%) of the TB cells and none of the SH cells had this low of FR ($P = 4.9 \times 10^{-9}$ and 6.1×10^{-7}, respectively; Fisher's exact test). Therefore, FR is highly diagnostic of SH versus TR cells independent from morphological analysis, but morphology is required to characterize with near 100% reliability.

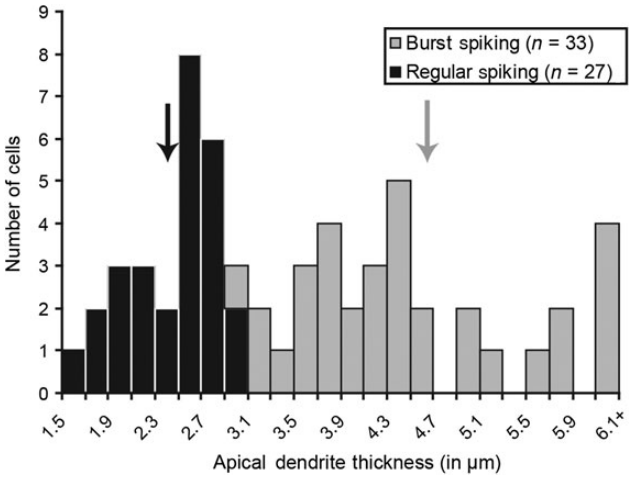

Figure 3. Distribution of the apical dendrite thickness between the tall pyramidal cells. Apical dendrite was measured at either the first spine or at the first branch point. Tall bursting cells had a significantly thicker apical dendrite than the tall regular-spiking cells. All 32 cells that had an apical dendrite above 3 μm were tall bursting cells. Arrows correspond to location of the mean apical dendrite thickness for that particular group (gray for burst spiking, black for regular spiking).

The most striking feature of TB pyramidal cells was AHPtr (see Materials and Methods), which is the ratio of the time interval between the peak and AHP to the interspike interval time. Since action potentials in TB cells were followed by a fast ADP (i.e., a rise in ΔEOS), this caused the AHP to occur later in the interspike interval. The AHPtr for TB cells was 0.488 (±0.008; Fig. 4C,D), which was significantly higher than those of TR cells (0.330 ± 0.007; $P = 1.9 \times 10^{-12}$, Mann–Whitney *U*-test) and for SH pyramidal cells (0.338 ± 0.013, $P = 9.5 \times 10^{-9}$, Mann–Whitney *U*-test). All of the TB cells had an AHPtr greater than 0.4, whereas only 1 SH cell and none of the TR cells met this criteria ($P = 3.4 \times 10^{-23}$, Fisher's exact test), which made it a better predictor of burst spiking than the ΔEOS measure. A combination of the apical dendrite diameter and AHPtr was the best predictor of whether a cell was a TB cell or a TR cell (Fig. 4D).

We found some more subtle differences between the spikes shapes of the 3 cell groups. For a summary of these results see Table 1.

In conclusion, we were able to differentiate our tall cells into 2 different populations based on their spiking patterns, electrophysiological properties, and morphological characteristics. TR cells had broader spikes, a more negative ΔEOS, more negative ΔAHP_1, and an AHP that occurred closer to the spike (low AHPtr), and they adapted slowly. TB cells had a higher FR and were characterized by having a fast ADP that would end their spike sooner (positive ΔEOS). As a result, their AHP occur much later (high AHPtr). Furthermore, we found further evidence that the SH cells, a population distinguished from the other 2 morphologically, has electrophysiological characteristics that are unique to it, including higher FR, more negative ΔEOS, and less negative ΔAHP_2.

Laminar Sources of Functional Excitatory Input

We used laser-scanning photostimulation to map local sources of excitatory input to all 84 layer 5 pyramidal cells. Complete tables of the photostimulation results for all of our cells are provided in Supplementary Tables 1–3, with sample excitatory input patterns for each cell type provided in Fig. 5.

As a whole, nearly all layer 5 neurons received significant input from all layers, and hence there was no significant difference between the cell types based on probability that a particular layer would provide significant input. Only 4 of the 84 cells (4.8%; 2 TR and 2 TB cells) did not receive significant input from layers 2/3, and 5 of 84 cells (6.0%; 2 SH cells, 1 TR cells, and 2 TB cells) did not receive input from layer 6. There were no significant differences between cell subtypes in this measure.

Nevertheless there were significant differences in the strength of excitatory input from certain layers between the SH cells and the 2 tall subtypes of pyramidal neurons. This was revealed by analysis of the relative strength of excitatory input from each layer to the 3 different types of cells. SH neurons received their strongest input from layer 4 (38.9 ± 4.5%; mean ± SEM) followed by layer 5 (34.8 ± 3.8%; Fig. 5A,B and 6A). Functional input from layer 2/3 and layer 6 was weaker, with layer 2/3 providing 17.0 ± 2.2% of EI and layer 6 providing 9.3 ± 1.8% input.

TR cells, on the other hand, received their strongest input from layer 5 (46.6 ± 3.0%; Figs 5C,D and 6A). This input was

Table 1: Spike analysis properties for different layer 5 cell types

Cell type	Short	Tall regular	Tall bursting
Resting membrane potential (in mV)	−53.36 ± 1.23	−52.04 ± 1.10	−52.48 ± 1.00
Input resistance (in MΩ)	$208.252^{a,c}$ ± 13.422	$160.757^{b,c}$ ± 9.265	$109.256^{a,b}$ ± 7.089
End of spike from threshold (ΔEOS, in mV)	$-3.042^{a,c}$ ± 0.465	$-1.511^{b,c}$ ± 0.422	$2.377^{a,b}$ ± 0.381
Half peak width (HPW, in ms)	2.010 ± 0.096	2.211^{b} ± 0.123	1.907^{b} ± 0.072
Afterspike hyperpolarization from threshold (ΔAHP_1, in mV)	-7.633^{c} ± 0.644	$-10.541^{b,c}$ ± 0.488	-6.970^{b} ± 0.639
Afterspike hyperpolarization from EOS (ΔAHP_2 in mV)	$-4.591^{a,c}$ ± 0.659	−9.030[c] ± 0.481	-9.347^{a} ± 0.749
Afterspike hyperpolarization time ratio (AHPtr)	0.338^{a} ± 0.013	0.330^{b} ± 0.007	$0.488^{a,b}$ ± 0.008
Firing rate (FR, in Hz)	$90.169^{a,c}$ ± 4.343	$29.318^{b,c}$ ± 4.391	$63.350^{a,b}$ ± 4.807
Adaptation coefficient	0.900 ± 0.026	0.825^{b} ± 0.021	0.903^{b} ± 0.011

[a]Significant difference ($P < 0.05$) between short pyramidal and tall burst spiking cells.
[b]Significant difference ($P < 0.05$) between tall regular and burst spiking cells.
[c]Significant difference ($P < 0.05$) between short pyramidal and tall regular-spiking cells. Mann–Whitney *U*-test. Values are mean ± SEM.

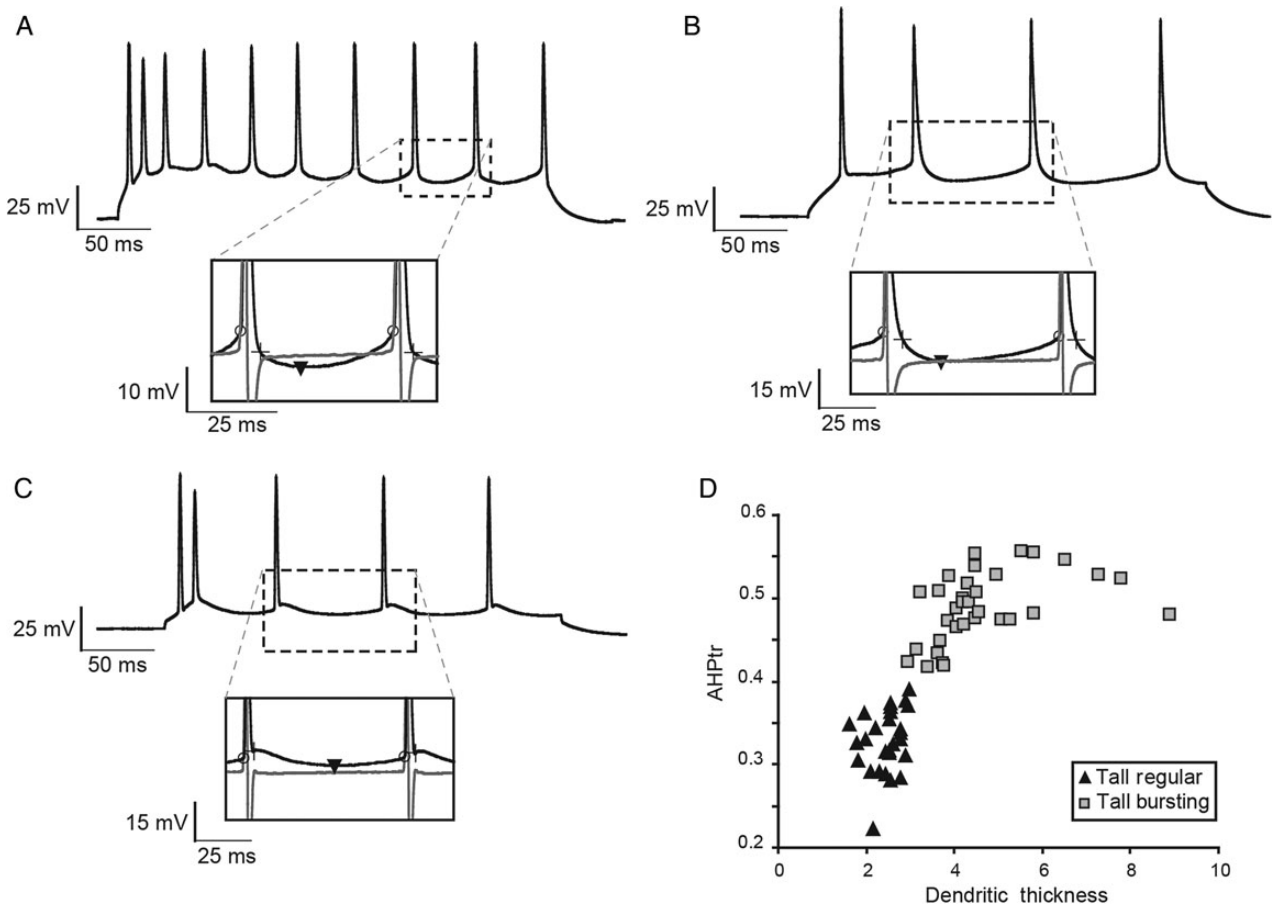

Figure 4. Spike properties of the three subtypes of layer 5 pyramidal neurons. (*A–C*) Example spike trains of 3 different subtypes with insets showing enlargements of the base of 2 spikes and interspike interval. In the insets, the threshold is represented by an open circle, the EOS as a plus sign, and the AHP as a black triangle. The gray line represents the first derivative (dV/dt) of the spike wave. (*A*) Spike train from a short pyramidal cell. These spikes are characterized by a higher FR, most negative ΔEOS, and least negative ΔAHP_2. Also their AHPtr was <0.4. (*B*) Spike train from a tall regular-spiking cell. These spikes are characterized by a low FR, slow adaptation, higher HPW, a negative ΔEOS, and the most negative ΔAHP_1. Similar to the short pyramidal cells, they also had a AHPtr that was <0.4. (*C*) Spike train from a tall bursting cell. These spikes are characterized by a high FR (caused by the burst), a positive ΔEOS and an AHPtr that was >0.4. (*D*) The relationship of the apical dendrite thickness and AHPtr. Tall bursting cells and tall regular-spiking cells can be clearly distinguished from each other using a combination of morphological and electrophysiological properties.

significantly greater than the layer 5 input to SH cells ($P = 0.01$, Mann–Whitney *U*-test). TR cells also received strong input from layer 4 (27.2 ± 2.7%), though this was significantly lower than the strength of input to the SH neurons ($P = 0.02$, Mann–Whitney *U*-test). Similar to SH cells, they received weaker input from layer 2/3 (12.2 ± 1.5%) and layer 6 (14.0 ± 2.0%). The input from these 2 latter layers was insignificantly different from those to the SH neurons.

The relative strength of laminar input to the TB cells was also significantly different from SH cells, but nearly identical to the

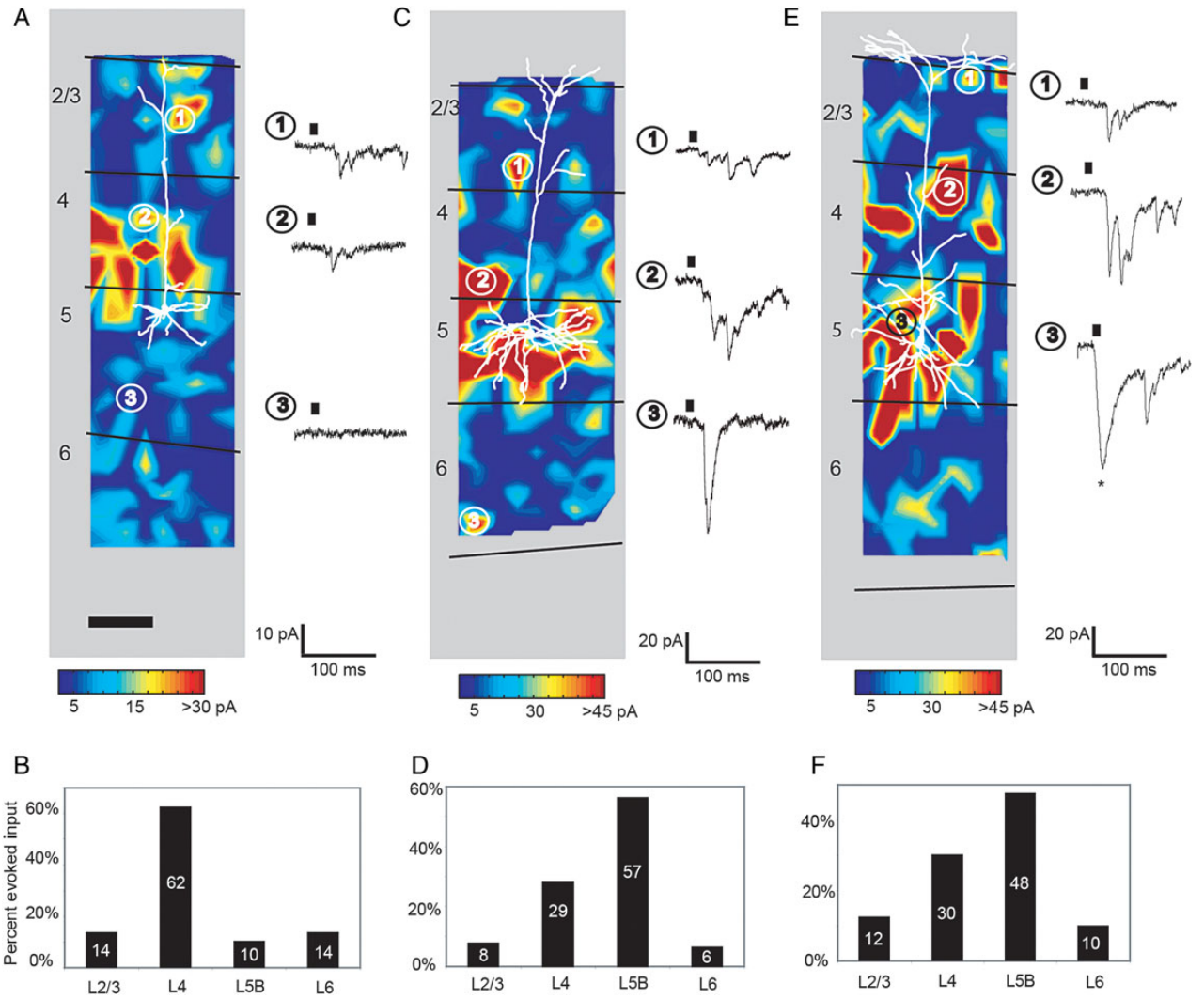

Figure 5. Examples of laminar excitatory input to 3 individual layer 5 pyramidal cells. Pseudo-colored input maps demonstrate representative patterns of excitatory input to 3 individual neurons. These input maps are linear interpolations of the sum of EPSC amplitude values (minus spontaneous EPSCs) measured following photostimulation at sites spaced ~50 µm apart. Colored horizontal scale bars indicate the corresponding sum of EPSC amplitude values for input maps above. Camera lucida drawings of dendrites (white lines) and soma (white) are overlaid onto plots. Gray areas are present so that neuronal processes can be seen against otherwise white background. Laminar borders are represented by horizontal black lines and labeled on the left. To the right of each input map are example voltage-clamp recordings (−65 mV holding potential) made while stimulating presynaptic regions signified by the corresponding circled numbers. Short dashes above each trace show the duration of photostimulation and onset of glutamate activation. The current marked with an asterisk (E3) shows a direct response to glutamate uncaging and is omitted from analysis. Percentage of evoked excitatory input (EI, see text) from each layer is illustrated in the bar graphs below each plot. (*A*) Short pyramidal neuron that received significant input from all layers. (*B*) Bar graph representing the percent of total evoked input from each layer for cell in (*A*). In this case, the strongest input came from layer 4 followed by layers 2/3 and 6. The weakest significant input came from layer 5. (*C*) Tall burst spiking pyramidal neuron that received significant input from all layers. (*D*) Bar graph representing the percent of total evoked input from each layer for cell in (*C*). In this case, the strongest input came from layer 5 followed by layer 4. (*E*) Tall regular-spiking pyramidal cell that received significant input from all layers. (*F*) Bar graph representing the percent of total evoked input from each layer for cell in (*E*). In this case, the strongest input was from layer 5 followed by layer 4. Black scale bar in (*A*) represents 200 µm.

values from the TR cells (Figs 5*E*,*F* and 6*A*). Similar to the TR cells, the TB cells received their strongest input from layer 5 (48.5 ± 2.4%). This was significantly different from the SH cells ($P = 0.01$, Mann–Whitney *U*-test) but not from the TR cells ($P = 0.91$, Mann–Whitney *U*-test). TB cells also received input from layer 4 (26.7 ± 1.9%) which was significantly different from SH neurons ($P = 0.03$, Mann–Whitney *U*-test), but not from TR cells ($P = 0.80$, Mann–Whitney *U*-test). Similar to TR and SH cells, TB cells received 12.2 ± 1.5% of their input from layer 2/3 and 14.0 ± 2.0% of their input from layer 6. These values were insignificantly different from the other cell types.

Since the values of the 2 tall cell types were very similar to each other, in a further analysis we grouped the 2 tall subtypes together and compared them with the SH cells. As expected, there was a significant difference between the SH and the tall pyramidal cells in the percent input they received from layer 4 ($P = 0.01$, Mann–Whitney *U*-test) and from layer 5 ($P = 6.2 \times 10^{-3}$, Mann–Whitney *U*-test). However, there was no significant difference between the 2 groups in the strength of input from layer 2/3 ($P = 0.12$, Mann–Whitney *U*-test) or layer 6 ($P = 0.12$, Mann–Whitney *U*-test).

For all cell types, we also calculated the ratio of layer 4 input to the total input from layers 4 and 5. For this value, a ratio of 1

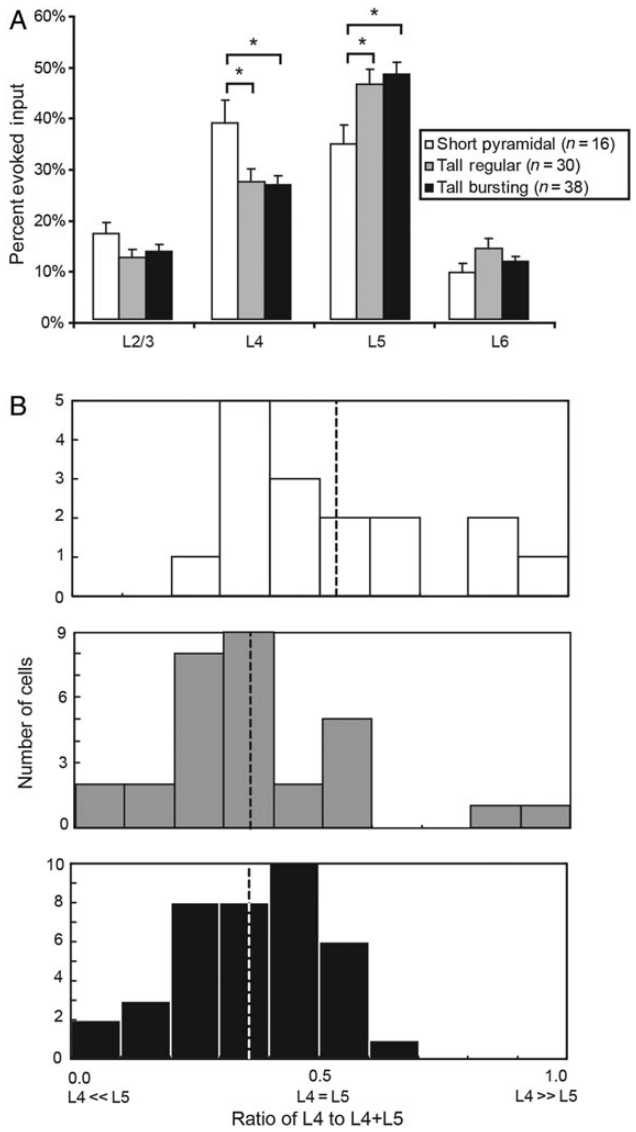

Figure 6. Laminar input to the 3 types of layer 5 neurons. (*A*) Mean ± SEM percent of total evoked input for each layer for the 3 subtypes of layer 5 cells. Short pyramidal neurons received a larger percentage of evoked input from layer 4 than other cell types (Mann–Whitney *U*-test, tall regular, $P < 0.05$, tall bursting, $P < 0.05$). However, they also received relatively weaker input from layer 5 than did the 2 tall cells (Mann–Whitney *U*-test, tall regular $P < 0.01$, tall bursting cells, $P < 0.05$). The inputs to the 2 tall cells were insignificantly different from each other. *Significance of $P < 0.05$. (*B*) Frequency bar graphs for each cell type showing the ratio of L4 input to total input from L4 and L5. A value near 1.0 (toward the left) implies that the cell received much more L4 input than L5; a value near 0 implies that the cell received much more L5 input than L5. Dashed lines indicate the mean of the distribution for each cell types. The means of the 2 tall populations are nearly identical, but the mean of the short pyramidal cells is shifted to the left.

would imply that the cell received input from layer 4 but not 5, a ratio of 0 would imply that the cell received input from layer 5 but not 4, and a ratio of 0.5 would imply that the cell received equal input from layers 4 and 5. The layer 4 input ratio for SH cells was 0.52 (±0.05) suggesting that they receive input evenly from layers 4 and 5 (see Fig. 6*B*). This ratio was significantly higher than that of TR cells (0.37 ± 0.03, $P = 0.02$, Mann–Whitney *U*-test) and the TB cells (0.37 ± 0.02, $P = 0.02$, Mann–Whitney *U*-test), and to the population of tall cells as a whole (0.37 ± 0.02, $P = 0.01$, Mann–Whitney *U*-test). Unlike SH cells, tall cells receive twice as much layer 5 input than they do from layer 4.

Common Input to Simultaneously Recorded Neurons

Because photostimulation with glutamate uncaging generates action potentials asynchronously within a small population of neurons near the stimulation site (Dantzker and Callaway 2000; Yoshimura and Callaway 2005; Yoshimura et al. 2005), it is possible to use the relative timing of evoked postsynaptic potentials recorded simultaneously in 2 different neurons (cross-correlation analysis) to infer what proportion of their inputs are shared versus arising from separate presynaptic neurons (Yoshimura and Callaway 2005; Yoshimura et al. 2005). Following photostimulation and recordings from 2 neurons, cross-correlation analyses are used to generate an estimate of shared input called CP (see Materials and Methods and Yoshimura and Callaway 2005; Yoshimura et al. 2005). The CP is an estimate of the proportion of shared input. Separate values for CP can be obtained for stimulation sites located in different cortical layers.

We tested 42 pairs of layer 5 cells (see Supplementary Tables 4 and 5), of which only one was a connected pair, a reciprocal connection between 2 TB cells. This low number of connected pairs is likely due to the older age of the rats used for the study and the proximity of the 2 cells (often <10 µm apart) from which we recorded (Song et al. 2005). Since the CP of connected cells can be higher than nonconnected cells, this pair was excluded from this part of the analysis (Yoshimura and Callaway 2005; Yoshimura et al. 2005). By comparing the CPs of pairs of layer 5 cells that were the same or different subtypes, we could deduce whether these 2 populations get input from different populations of pyramidal cells. That is, if TR cells are indeed a different population of cells than TB cells, then they might share input from the same presynaptic cells (and have a higher CP) than when they are paired with a different cell type.

We were able to compute the layer 5 CP of 8 pairs of TR cells (TR-TR) and 13 pairs where a TR cell was paired with a cell of another type (TR-X). On average, the layer 5 CP of TR-TR pairs was 0.079 ± 0.008 (mean ± SEM; 8 pairs, Fig. 7*A*), which means that for 7.9% of cases in which a layer 5 neuron was photostimulated and evoked an EPSC in one TR cell, that same layer 5 neuron also evoked a synchronous EPSC that was detected in the other TR cell. This CP value was significantly higher than that of TR-X pairs (CP = 0.022 ± 0.009; $P = 5.1 \times 10^{-4}$, Mann–Whitney *U*-test). We also calculated the layer 6 CP for TR-TR pairs (Fig. 7*C*). These pairs had a relatively high CP (0.055 ± 0.019) that was nearly significantly different from TR-X pairs (0.006 ± 0.020; $P = 0.08$, Mann–Whitney *U*-test). TR-TR pairs therefore have a higher CP, and hence have a higher proportion of shared presynaptic neurons from within layer 5 and possibly from layer 6, compared with their unmatched counterparts. We were not able to detect any significant differences between the CP of the TR-TR pairs and TR-X pairs for stimulation sites in the superficial layers.

We were also able to compute the layer 5 CP of 11 pairs of TB cells (TB-TB; excluding one connected pair—see above) and 13 pairs where a TB cell was matched with another cell type (TB-X cells; Fig. 7*A*). On average, the layer 5 CP for TB-TB pair was 0.070 ± 0.013 which was also significantly higher from the TB-X pairs (0.032 ± 0.007; $P = 0.03$, Mann–Whitney *U*-test). TB-TB pairs did not have any significant differences between their layer 6 CP and those found for TB-X pairs (0.032 ± 0.010 for TB-TB pairs and 0.017 ± 0.017 for TB-X cells, $P = 0.15$; Fig. 7*C*). However, TB-TB pairs had a significantly higher CP from layer 4 compared

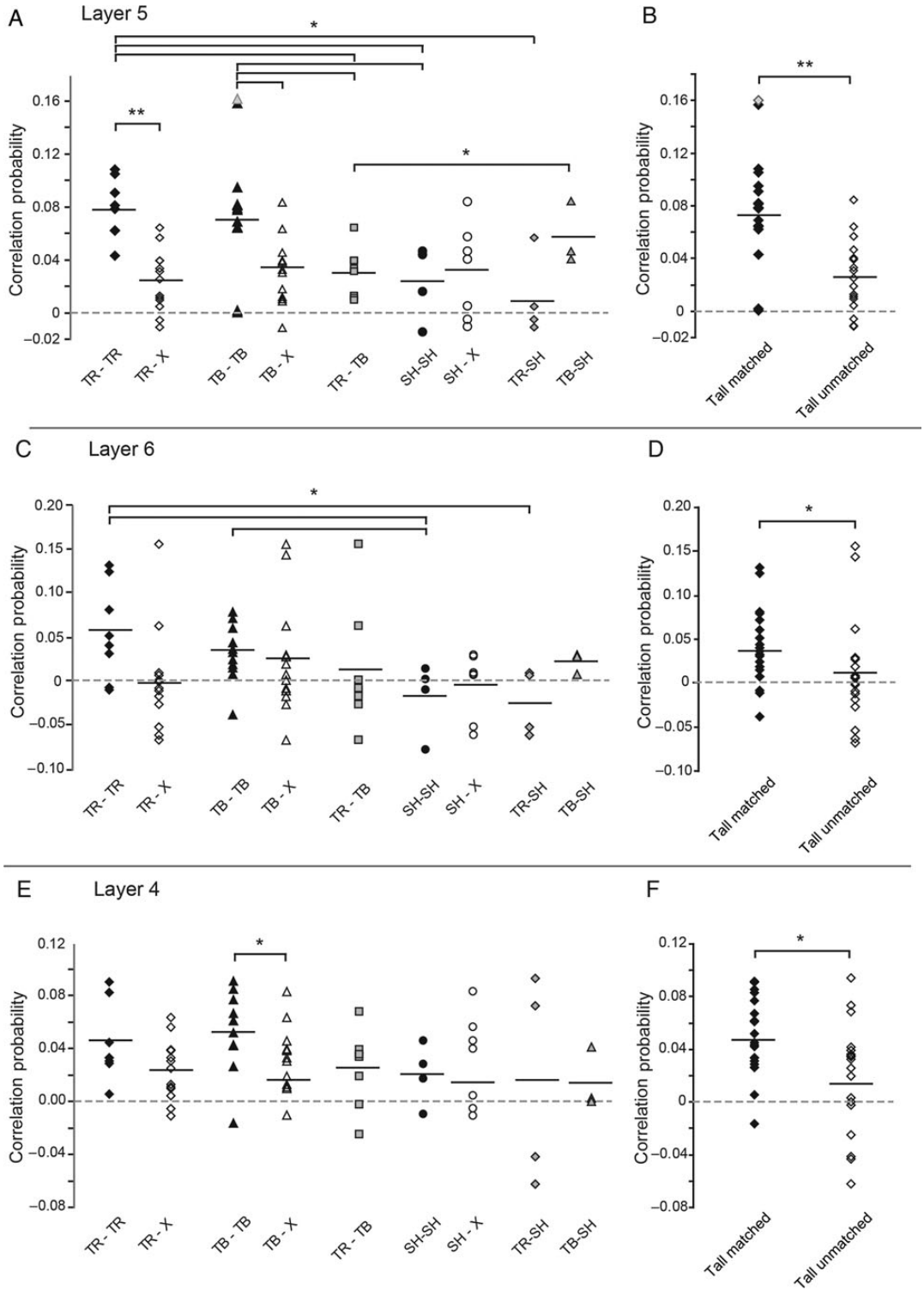

Figure 7. Correlation probabilities for different cell groups. (*A*) There are significant differences in the correlation probability (CP) from layer 5 between matched tall regular-spiking cells (TR-TR) and their respective unmatched cohorts (TR-X; $P < 0.001$) and also matched tall spiking cells (TB-TB) and their respective unmatched cohorts (TB-X; $P < 0.05$). There were no significant difference between matched short pyramidal cells (SH-SH) and their respective unmatched cohorts (SH-X). (*B*) There was a significant overall effect between matching pairs of tall cells (TR-TR and TB-TB) and unmatched tall cells (TR-X or TB-X; $P < 0.05$). (*C*) Within layer 6, there are significant difference in CP between matched tall regular-spiking cells (TR-TR) and matched and short pyramidal cells (SH-SH; $P < 0.05$) and tall regular-spiking cells and short pyramidal cells (TR-SH; $P < 0.05$). Matched tall bursting cells (TB-TB) were significantly different from matched short pyramidal cells (SH-SH; $P < 0.05$). (*D*) In layer 6, there was a significant overall effect between matching pairs of tall cells (TR-TR and TB-TB) and unmatched tall cells (TR-X or TB-X; $P < 0.05$). (*E*) Within layer 4, there was only a significant difference between matched tall bursting cells (TB-TB) and unmatched tall bursting cells (TB-X; $P < 0.05$). (*F*) In layer 4, there was a significant overall effect between matching pairs of tall cells (TR-TR and TB-TB) and unmatched tall cells (TR-X or TB-X; $P < 0.05$). Note: * implies $P < 0.05$; ** implies $P < 0.001$.

with TB-X pairs (0.052 ± 0.009 for TB-TB pairs, 0.023 ± 0.007 for TB-X pairs, $P = 0.03$, Mann–Whitney U-test; Fig. 7E). We could not detect any other significant differences between the CP from the other layers of TB-TB pairs and those found for TB-X cells.

The above observations suggest that particular subpopulations of cells within layers 5 and/or layer 4 or 6 (likely different cell types of unknown identity) selectively provide excitatory input to TR or TB cells versus other cell types. But the grouping of all non-TR or non-TB cells in the above analyses does not allow a distinction between whether TR cells receive different inputs than TB cells, versus the possibility that TR and TB cells receive similar inputs but different from the remaining cell types. We therefore directly compared matching pairs of tall cells (TR-TR or TB-TB cells) with unmatched pairs of tall cells (TR-TB). Of the TR-X cell pairs (see above), 8 pairs were TR-TB cells with a layer 5 CP of 0.030 ± 0.007. The TR-TR cell pair CP (0.079 ± 0.008) was significantly higher than TR-TB cell pairs (0.030 ± 0.007, $P = 0.0023$, Mann–Whitney U-test), as was the CP of TB-TB pairs (0.070 ± 0.013, $P = 0.02$, Mann–Whitney U-test).

Next, we pooled data from all the tall matching pairs (TR-TR and TB-TB; $n = 19$) and compare them with all tall, unmatched pairs (TB-X or TR-X cells; $n = 18$). Tall matching pairs had significantly higher CPs from layer 5 than unmatched pairs (0.074 ± 0.008 for matched tall pairs, 0.027 ± 0.006 for unmatched tall pairs; $P = 7.0 \times 10^{-5}$, Mann–Whitney U-test, Fig. 7B). This was also true for layer 6 (0.042 ± 0.010 for tall matched, 0.010 ± 0.014 for tall unmatched; $P = 0.02$ Mann–Whitney U-test; Fig. 7D) and also layer 4 (0.049 ± 0.007 for tall matched, 0.018 ± 0.010 for tall unmatched; $P = 0.05$ Mann–Whitney U-test; Fig. 7F). We then compared the tall matched pairs with a subset of the tall unmatched where both cells were tall (TR-TB; $n = 8$). We also found a significant difference in layer 5 CP between these 2 populations ($P = 1.5 \times 10^{-3}$, Mann–Whitney U-test). Although there was no significant difference in CP from layer 6 ($P = 0.13$) or layer 4 ($P = 0.15$), this was the only time we found a significant difference in CP from layer 2/3 (0.037 ± 0.011 for tall matched, 0.020 ± 0.007 for TR-TB; $P = 0.04$ Mann–Whitney U-test).

Interestingly, SH–SH pairs (4 pairs) did not have as high of a CP as their matching tall counterparts. Their layer 5 CP was 0.022 ± 0.014 which was insignificantly different from that of SH cells matched with some other cell type (SH-X; $n = 7$ pairs; 0.031 ± 0.013; $P = 0.63$, Mann–Whitney U-test; Fig. 7A) but was significantly lower than that of tall matched pairs ($P = 0.01$, Mann–Whitney U-test). Furthermore, no significant differences existed between SH–SH and SH-X cells in CP from other layers. The low CP from layer 5 for SH–SH pairs differed significantly from those of each of the tall matched pairs and also the pooled tall matched pairs (TR-TR vs. SH-SH $P = 0.01$; TB-TB vs. SH-SH $P = 0.04$; and tall matched vs. SH-SH $P = 0.01$; Mann–Whitney U-test; Fig. 7A). The CP from layers 4 and 6 trended toward significance when compared with those of the matched tall pairs (layer 4 CP to tall matched vs. SH-SH $P = 0.09$; layer 6 CP to tall matched vs. SH-SH $P = 0.06$).

Finally, we noticed a subtle difference in CP when we took a closer look at pairs of SH cells and the tall subtypes. As expected, TR-TR pairs have a significantly higher CP from layer 5 when compared with TR-SH pairs (0.011 ± 0.015, $P = 8.0 \times 10^{-3}$, Mann–Whitney U-test); however, there was no significant difference between TB-SH pairs (0.057 ± 0.014) and TB-TB pairs ($P = 0.58$, Mann–Whitney U-test). Furthermore, there was no significant difference between TR-SH pairs to TR-TB pairs ($P = 0.13$, Mann–Whitney U-test), but there was a significant difference between TB-SH pairs and TR-TB pairs ($P = 0.04$, Mann–Whitney U-test). This suggests that TB-SH pairs are 5 times more likely to receive input from the same cells in layer 5 than are TR-SH pairs. There was no difference between TR-SH ($n = 4$) and TB-SH ($n = 3$) pairs, though there were too few numbers of these pairs to make an adequate comparison ($P = 0.15$, Mann–Whitney U-test).

Discussion

Our analysis of the morphological and electrophysiological properties of layer 5 pyramidal neurons in rat visual cortex revealed that they can be divided into 3 subtypes (SH, TR, TB). In the rat visual cortex, bursting cells with thick apical dendrites that are similar to our TB cells have been described previously (Hallman et al. 1988; Chagnac-Amitai et al. 1990; Larkman and Mason 1990; Kasper et al. 1994). Likewise, in other areas of neocortex, bursting cells with thick apical dendrites are corticothalamic projecting cells (Morishima and Kawaguchi 2006; Hattox and Nelson 2007). Cells with similar morphology and firing pattern have been described in the mouse somatosensory cortex where they have also been characterized as being corticotectal/corticothalamic cells (Larsen and Callaway 2006; Brown and Hestrin 2009). However, earlier studies of the rat visual cortex have grouped RS cells (i.e., TR and SH cells) together (Hallman et al. 1988; Kasper et al. 1994). Only recently have TR and SH cells been characterized as distinct groups. Given their morphological and electrophysiological similarity to cells in the mouse and rat somatosensory cortex, as well as the rat prefrontal cortex, these cells are likely corticocortical projecting neurons (Morishima and Kawaguchi 2006; Hattox and Nelson 2007; Larsen et al. 2007).

In addition to our anatomical findings, we identified the laminar sources of functional excitatory input to individual neurons (Fig. 8). Although these cells likely received additional input to the distal dendrites, some of which may have been attenuated by IPSCs where isopotentiality could not be established with our voltage clamp, the focus of the study was to measure EPSCs at the cell soma where they could have an influence on whether the cell fires action potentials.

SH neurons received input mainly from layer 4, with almost the same strength of input from layer 5. The 2 tall subtypes of layer 5 neurons, on the other hand, had identical input patterns. Both received the strongest input from layer 5 followed by layer 4. The tall cells received nearly twice as much input from layer 5 than they did from layer 4. All cells received weaker but significant input from layers 2/3 and 6.

Previous paired recording studies of layer 2/3 and layer 5 suggested that the probability that a layer 2/3 cell was connected to a layer 5 RS cell was 1/40 (Thomson and Bannister 1998). However, this probability increased to one-fourth for layer 2/3 cells connected to layer 5 burst spiking cells. Since our study found that the strength of input (or the sum of EPSCs) from layer 2/3 to both tall subgroups are not significantly different (Fig. 6A, Supplementary Tables 2 and 3), this could be because either many layer 2/3 synapses onto layer 5 bursting cells form relatively weak connections, or the layer 2/3 synapses onto layer 5 RS cells make relatively strong connections.

Our study is not the only photostimulation study of layer 5 pyramidal neurons. Schubert et al. (2001, 2006) distinguished between 2 cell types in the rat somatosensory cortex, the intrinsically burst spiking cells (IB) and RS cells. Their results are very similar to our findings; both cell types received widespread input from layers 5 and 4, less widespread input from layer 2/3, and with little difference between the 2 cell populations in the level of input from these layers. A key difference is that, although RS cells received the least widespread input from layer 6 (similar to both populations of our tall pyramidal cells), the IB cells received their most widespread input from layer 6. The most likely explanation for the differences

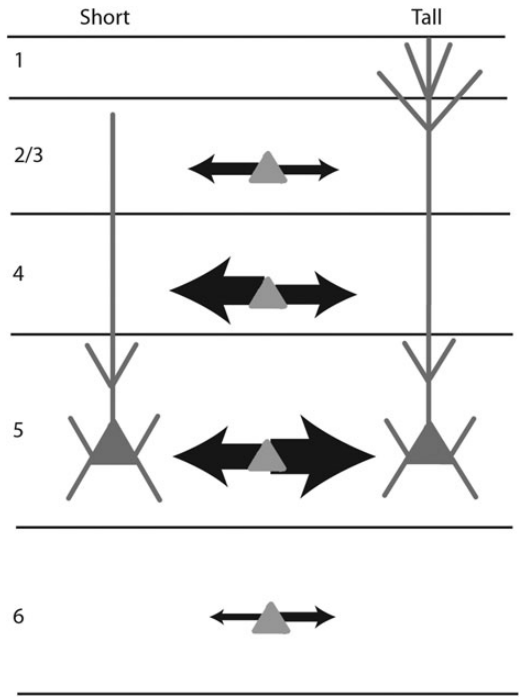

Figure 8. Schematic diagram summarizing the local input to short and tall pyramidal cells of layer 5. Thickness of black arrows represents the strength and directionality of the source of local excitatory input to the 2 different cell subtypes. Short pyramidal cells receive significant local input from all layers. The inputs from layers 2/3 and 6 are weaker than those from layers 4 and 5. Short cells receive stronger input from layer 4 than they do from layer 5. Tall pyramidal cells also receive significant local input from all layers. Like short cells they receive weaker input from layers 2/3 and 6 than they do from layer 4 and 5. However, a key difference between the 2 cell types is that tall cells receive stronger layer 5 input than they do from layer 4.

in laminar input is that there are some key differences in the circuitry of the 2 sensory cortices. A more recent photostimulation study of the rat somatosensory cortex reported a prominent layer 2/3 to layer 5 input (Hooks et al. 2011). However, their figures show stronger input from layer 4, and the layer 2/3 depth appears to be twice as large as layer 4. Unfortunately, an analysis of input to morphological subtypes was not done.

Layer 5 pyramidal cell subtypes are the only ones described in the photostimulation literature that do not have significant differences in local interlaminar input. Nevertheless, using paired recordings and cross-correlation analyses, we tested for differences in local excitatory inputs to each cell type that are organized at a finer spatial scale (e.g., cell types or individual neurons) than cortical layers. CP is a measure of synchronous EPSCs in a pair of neurons, and a predictor of the proportion of shared presynaptic neurons between them. TR cells receive more than 3 times as much common input from layer 5 when they are matched up with another unconnected TR cell. This observation was also true for TB cells; when they were matched with another unconnected TB cell, they received more than twice as much shared input from layer 5. Interestingly, we did not observe the same trend in the layer 5 CP of the matched pairs of SH neurons.

We also found differences in CP from other layers. Matched TR cells receive nearly 10 times more common input from within layer 6 compared with unmatched TR cells. However, matched TB cells did not have a significant difference in layer 6 CP. Matched TB cells, though, shared twice as much common input from layer 4 compared with unmatched TB cells. However, matched TR cells did not have a significant difference in their layer 4 CP. Furthermore, tall pyramidal layer 5 cells shared 20 times more common input from layer 2/3 when paired with a matching cell subtype than when paired with unmatching tall pyramidal cells. Our inability to find a more robust layer 2/3 CP may be that the L2/3 cells appear to be selectively connected to connected pairs of layer 5 pyramidal neurons (Kampa et al. 2006). Finally, common input was not only observed for cell pairs that were of the same subtype; TB cells were twice as likely to share common input with SH cells than when they were paired with TR cells.

Our CPs are quite low when compared with the ones found in connected pairs of layer 2/3 neurons (Yoshimura and Callaway 2005; Yoshimura et al. 2005). The high CP between connected cells in the layer 2/3 of the rat visual cortex suggests a fine-scale specificity in the network of these cells. These high values were only observed, however, when the recorded layer 2/3 cell pairs were directly connected to each other. Because we sampled unconnected pairs, our experiments cannot determine whether similarly high proportions of shared input might be found for connected layer 5 cell pairs. But the values for shared input to connected neurons in layer 5 of rat somatosensory cortex following stimulation of single layer 2/3 pyramids strongly suggests that such an organization does not exist, at least between layers 2/3 and 5 (Kampa et al. 2006). Further studies are required to identify the extent of shared input from other cortical layers onto connected layer 5 pyramidal neuron pairs.

Previous studies of layer 5 in the rat prefrontal cortex show that there are selective connections between different cell types (Morishima et al. 2011; Otsuka and Kawaguchi 2011). For example, cells equivalent to our TR cells synapse onto other TR cells and to cells corresponding to our TB with similar frequency (~10% probability of connection). However, the TB cells rarely synapse onto the TR cells (~1%). This finding, along with the differences in CP we observed depending on the types of layer 5 pyramids recorded simultaneously in our study, implies that selective connections between different types of layer 5 pyramidal cells is also present in the rat visual cortex. Nevertheless, more direct identification of the presynaptic cell types providing EI in the rat visual cortex would be required for definitive proof.

Although the lack of recordings from connected layer 5 pyramidal neuron pairs in our study left us unable to assess the nature of fine-scale specificity in layer 5 of the rat visual cortex, other pieces of evidence strongly suggest that it does exist (Song et al. 2005; Kampa et al. 2006). The extent to which connectional motifs relate to differences in rates of connectivity between different cell types (Morishima et al. 2011; Otsuka and Kawaguchi 2011), versus fine-scale subnetworks of neurons of the same type (Song et al. 2005; Yoshimura and Callaway 2005; Yoshimura et al. 2005; Kampa et al. 2006) remains unknown.

In conclusion, we find evidence for at least 3 different morphological and physiological subtypes of layer 5 pyramidal neurons in the rat visual cortex. These cell types all pool significant excitatory input from across all the cortical layers and have significant differences in the strengths and proportions of their input that they receive from those layers. Finally, layer 5 neurons of the same types tend to receive more common input from subpopulations of neurons than cell pairs of different types, likely reflecting a tendency for different types of cortical cells to connect selectively to each type of layer 5 pyramid.

Supplementary Material

Supplementary material can be found at: http://www.cercor.oxfordjournals.org/.

Funding

This work was supported by National Institute of Health (EY-010742 and MH-063912 to E.M.C.; GM-007198 to A.Z.).

Notes

We acknowledge Takuma Mori and Aryn Gittis for their generous help with the spike analysis, and Rose Z. Jones for helping analyze a significant portion of the data collected for this study. *Conflict of Interest*: None declared.

References

Aertsen AM, Gerstein GL, Habib MK, Palm G. 1989. Dynamics of neuronal firing correlation: modulation of "effective connectivity". J Neurophysiol. 61:900–917.

Briggs F, Callaway EM. 2001. Layer-specific input to distinct cell types in layer 6 of monkey primary visual cortex. J Neurosci. 21:3600–3608.

Briggs F, Callaway EM. 2005. Laminar patterns of local excitatory input to layer 5 neurons in macaque primary visual cortex. Cereb Cortex. 15:479–488.

Brown SP, Hestrin S. 2009. Intracortical circuits of pyramidal neurons reflect their long-range axonal targets. Nature. 457:1133–1136.

Callaway EM, Katz LC. 1993. Photostimulation using caged glutamate reveals functional circuitry in living brain slices. Proc Natl Acad Sci USA. 90:7661–7665.

Chagnac-Amitai Y, Luhmann HJ, Prince DA. 1990. Burst generating and regular spiking layer 5 pyramidal neurons of rat neocortex have different morphological features. J Comp Neurol. 296:598–613.

Dantzker JL, Callaway EM. 2000. Laminar sources of synaptic input to cortical inhibitory interneurons and pyramidal neurons. Nat Neurosci. 3:701–707.

de Kock CP, Bruno RM, Spors H, Sakmann B. 2007. Layer- and cell-type-specific suprathreshold stimulus representation in rat primary somatosensory cortex. J Physiol. 581:139–154.

Hallman LE, Schofield BR, Lin CS. 1988. Dendritic morphology and axon collaterals of corticotectal, corticopontine, and callosal neurons in layer V of primary visual cortex of the hooded rat. J Comp Neurol. 272:149–160.

Hattox AM, Nelson SB. 2007. Layer V neurons in mouse cortex projecting to different targets have distinct physiological properties. J Neurophysiol. 98:3330–3340.

Hooks BM, Hires SA, Zhang YX, Huber D, Petreanu L, Svoboda K, Shepherd GM. 2011. Laminar analysis of excitatory local circuits in vibrissal motor and sensory cortical areas. PLoS Biol. 9:e1000572.

Kampa BM, Letzkus JJ, Stuart GJ. 2006. Cortical feed-forward networks for binding different streams of sensory information. Nat Neurosci. 9:1472–1473.

Kasper EM, Larkman AU, Lubke J, Blakemore C. 1994. Pyramidal neurons in layer 5 of the rat visual cortex. I. Correlation among cell morphology, intrinsic electrophysiological properties, and axon targets. J Comp Neurol. 339:459–474.

Katz LC, Dalva MB. 1994. Scanning laser photostimulation: a new approach for analyzing brain circuits. J Neurosci Methods. 54:205–218.

Larkman A, Mason A. 1990. Correlations between morphology and electrophysiology of pyramidal neurons in slices of rat visual cortex. I. Establishment of cell classes. J Neurosci. 10:1407–1414.

Larsen DD, Callaway EM. 2006. Development of layer-specific axonal arborizations in mouse primary somatosensory cortex. J Comp Neurol. 494:398–414.

Larsen DD, Wickersham IR, Callaway EM. 2007. Retrograde tracing with recombinant rabies virus reveals correlations between projection targets and dendritic architecture in layer 5 of mouse barrel cortex. Front Neural Circuits. 1:5.

Mercer A, West DC, Morris OT, Kirchhecker S, Kerkhoff JE, Thomson AM. 2005. Excitatory connections made by presynaptic cortico-cortical pyramidal cells in layer 6 of the neocortex. Cereb Cortex. 15:1485–1496.

Morishima M, Kawaguchi Y. 2006. Recurrent connection patterns of corticostriatal pyramidal cells in frontal cortex. J Neurosci. 26:4394–4405.

Morishima M, Morita K, Kubota Y, Kawaguchi Y. 2011. Highly differentiated projection-specific cortical subnetworks. J Neurosci. 31:10380–10391.

Otsuka T, Kawaguchi Y. 2011. Cell diversity and connection specificity between callosal projection neurons in the frontal cortex. J Neurosci. 31:3862–3870.

Sawatari A, Callaway EM. 1996. Convergence of magno- and parvocellular pathways in layer 4B of macaque primary visual cortex. Nature. 380:442–446.

Schubert D, Kotter R, Luhmann HJ, Staiger JF. 2006. Morphology, electrophysiology, and functional input connectivity of pyramidal neurons characterizes a genuine layer Va in the primary somatosensory cortex. Cereb Cortex. 16:223–236.

Schubert D, Staiger JF, Cho N, Kotter R, Zilles K, Luhmann HJ. 2001. Layer-specific intracolumnar and transcolumnar functional connectivity of layer V pyramidal cells in rat barrel cortex. J Neurosci. 21:3580–3592.

Song S, Sjostrom PJ, Reigl M, Nelson S, Chklovskii DB. 2005. Highly nonrandom features of synaptic connectivity in local cortical circuits. PLoS Biol. 3:e68.

Thomson AM, Bannister AP. 1998. Postsynaptic pyramidal target selection by descending layer III pyramidal axons: dual intracellular recordings and biocytin filling in slices of rat neocortex. Neuroscience. 84:669–683.

West DC, Mercer A, Kirchhecker S, Morris OT, Thomson AM. 2006. Layer 6 cortico-thalamic pyramidal cells preferentially innervate interneurons and generate facilitating EPSPs. Cereb Cortex. 16:200–211.

Xu X, Callaway EM. 2009. Laminar specificity of functional input to distinct types of inhibitory cortical neurons. J Neurosci. 29:70–85.

Yabuta NH, Callaway EM. 1998a. Cytochrome-oxidase blobs and intrinsic horizontal connections of layer 2/3 pyramidal neurons in primate V1. Vis Neurosci. 15:1007–1027.

Yabuta NH, Callaway EM. 1998b. Functional streams and local connections of layer 4C neurons in primary visual cortex of the macaque monkey. J Neurosci. 18:9489–9499.

Yoshimoto S, Loo TM, Atarashi K, Kanda H, Sato S, Oyadomari S, Iwakura Y, Oshima K, Morita H, Hattori M, et al. 2013. Obesity-induced gut microbial metabolite promotes liver cancer through senescence secretome. Nature. 499:97–101.

Yoshimura Y, Callaway EM. 2005. Fine-scale specificity of cortical networks depends on inhibitory cell type and connectivity. Nat Neurosci. 8:1552–1559.

Yoshimura Y, Dantzker JL, Callaway EM. 2005. Excitatory cortical neurons form fine-scale functional networks. Nature. 433:868–873.

Zarrinpar A, Callaway EM. 2006. Local connections to specific types of layer 6 neurons in the rat visual cortex. J Neurophysiol. 95:1751–1761.